J Mater Sci (2007) 42:5327–5334
DOI 10.1007/s10853-006-0963-1

Effect of strain rate and environment on the mechanical properties of the Ni–19Si–3Nb–0.15B–0.1C intermetallic alloy at high temperatures

C. C. Fu · J. S. C. Jang · L. J. Chang · T. Y. Lin · C. M. Kuo

Received: 20 September 2005 / Accepted: 11 September 2006 / Published online: 29 March 2007

Abstract The effect of strain rate and environment on the mechanical behavior at different temperatures of the Ni–19Si–3Nb–0.15B–0.1C alloy is investigated by atmosphere-controlled tensile testing under various conditions at different strain rates and different temperatures). The results reveal that the Ni–19Si–3Nb–0.15B–0.1C alloy exhibits ductile mechanical behavior (UTS ~ 1250 MPa, $\varepsilon \sim 14\%$) at temperatures below 873 K under different atmosphere conditions. However, the alloy without boron and carbon addition shows ductile mechanical behavior only when the sample is tested in vacuum. This indicates that the microalloying of boron and carbon does overcome the environmental embrittlement from water vapor at test temperatures below 873 K for the Ni–19Si–3Nb base alloy. However, the boron and carbon doped alloy still suffers from embrittlement associated with oxygen at a medium high temperature (i.e. 973 K). In parallel, both of the ultimate tensile strength and elongation exhibit quite insensitive response with respect to the loading strain rate when tests are held at temperatures below 873 K. However, the ultimate tensile strength exhibits high dependence on the strain rate in air at temperatures above 873 K, decreasing the ultimate tensile strength with decreasing strain rate.

C. C. Fu · J. S. C. Jang (✉) · L. J. Chang · T. Y. Lin
Department of Materials Science & Engineering, I-Shou University, Kaohsiung, Taiwan, ROC
e-mail: scjang@isu.edu.tw

C. M. Kuo
Department of Mechanical and Automation Engineering, I-Shou University, Kaohsiung, Taiwan, ROC

Introduction

The intermetallic alloy based on Ni_3Si has been considered to be a candidate as high-temperature structural materials (especially for chemical plants), because Ni_3Si presents an increasing yield strength with temperature and shows excellent corrosion resistance over a wide range of temperature [1–3]. However, similar to Ni_3Al [4], the binary Ni_3Si suffers from environmental embrittlement at room temperature, which is exacerbated at the presence of hydrogen. Increasing the nickel content or adding the titanium has been reported to improve the room temperature ductility of the Ni_3Si-based alloys [5–7]. Likewise, the addition of Nb has also been reported to improve the room temperature ductility and strength [8–10]. To further improve the mechanical and related properties of the Ni_3Si based alloys, microalloying with a small amount of interstitial elements such as boron, carbon, or beryllium has been successfully applied to improve the room-temperature ductility for these $L1_2$ structured alloys [11–16]. However, these Ni_3Si-based alloys with a low percentage of interstitial atoms have also been reported to suffer from environmental embrittlement at elevated temperatures [6, 11, 12, 17–21]. The present study is launched to further understand the dependence of temperature and strain rate on environmental embrittlement of the Ni–19Si–3Nb–0.15B–0.1C alloy over a range of temperatures in different environments including air, vacuum and pure water vapor.

Experimental

The Ni_3Si based alloys, with compositions of Ni–19%Si–3%Nb (in atomic percent, at%, corresponding to Ni–9.9%Si–5.17%Nb in weight percent, wt%) and

Ni–19%Si–3%Nb–0.15%B–0.1%C (in at% corresponding to Ni–9.9%Si–5.17%Nb–0.03%B–0.02%C in wt%), were prepared by arc melting the appropriate amounts of carbonyl nickel, electronic grade silicon, 99.9% pure niobium, and 99.9% pure silicon carbide before drop casting into a cold copper mold. The composition-loss ratio of elements was less than 0.02 wt%, as determined by glowing discharge spectrum analysis; hence, the weight loss of the alloy during melting can be neglected. These ingots were annealed at 1080 °C for 24 h and aged at 700 °C for 10 h in a vacuum of 5×10^{-5} torr, and then machined into tensile specimens with a gauge section of 3 mm in width, 2 mm in thickness and 20 mm in length by electro-discharge machining. To prevent specimen surface damage, the specimen was carefully polished to reach a roughness of 25 μm. Tensile testing was performed at various temperatures ranging from room temperature to 800°C at different constant crosshead speeds with initial strain rates from 8×10^{-5} to 2×10^{-2} s^{-1}. All of these tests were designed to be conducted in different environments including air (with a humidity level of 60% RH), vacuum (with an environmental pressure less than 2×10^{-4} torr), and water vapor (with the water content about 850 ppm). For tests performed in water vapor, a vacuum (less than 2×10^{-4} torr) was achieved first in the test chamber prior to backfilling with distilled water.

The microstructure for each alloy and the fractured surface after testing were examined using a Hitachi scanning electron microscope (SEM), model S-2700, operating at 15 kV with energy dispersive spectrometry capability. In addition, samples for observation of the polished surface were metallographically prepared and etched with Marble's etching solution ($HCl_{(aq)}$ 50 mL + $CuSO_{4(s)}$ 10 grams + $H_2O_{(l)}$ 50 mL). The element distributions were examined and analyzed by electron probe micro-analysis (EPMA) with a Joel Microlab 310-D Scanning Auger Microprobe.

Results

Microstructures

The SEM image in Fig. 1a shows the heat-treated microstructure of Ni–19Si–3Nb base alloy, which contains dendrite of the β phase ($L1_2$ Ni_3Si), α (fcc solid solution)-β eutectic and many plate-like precipitates dispersed in the β matrix. This result is analogous to the report of Jang et al. [14, 15]. However, those plate-like precipitates change to small equiaxed precipitates for the microalloyed Ni–19Si–3Nb–0.15B–0.1C alloy are shown in Fig. 1b. The mapping images of different elements including Si, Ni, B, C for the Ni–19Si–3Nb–0.15B–0.1C alloy are shown in Fig. 2(c–f),

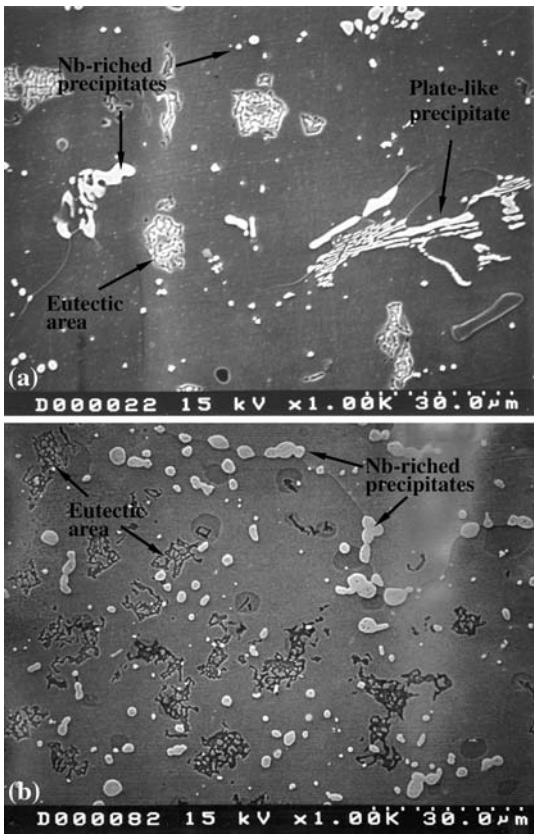

Fig. 1 The SEM metallographs of the Ni–19Si–3Nb alloy and Ni–19Si–3Nb–0.15B–0.1C alloy

respectively. The Nb and Si elements are mainly distributed in the precipitates as shown in Fig. 2(c, d). These Nb-riched precipitate was confirmed to be the cubic Nb_3Ni_2Si phase in our previous study [9, 14–16]. In addition, the microalloying of boron was revealed to segregate around these precipitates as indicated in Fig. 2e. This finding agrees well with those reported by Jang et al. [9, 14–16] and Liu et al. [13]. Jang et al. [14, 15] suggested that boron intends to segregate on the interface between the Nb_3Ni_2Si precipitates and β phase to reduce the surface energy of precipitates. This may explain the morphology change of Nb_3Ni_2Si precipitates by microalloying of boron into the Ni–19Si–3Nb based alloys.

Effects of loading temperature on the tensile properties

The variations of the yield stress (defined at 0.2%-offset strain) of the Ni–19Si–3Nb alloys with and without boron and carbon additions as a function of testing temperature are shown in Fig. 3. The yield stresses curves for the Ni–19Si–3Nb base alloy and the Ni–19Si–3Nb–0.15B–0.1C alloy, as presented by the dash and solid lines in Fig. 3, respectively, show a similar trend. Both curves show that the yield stress increases gradually with increasing

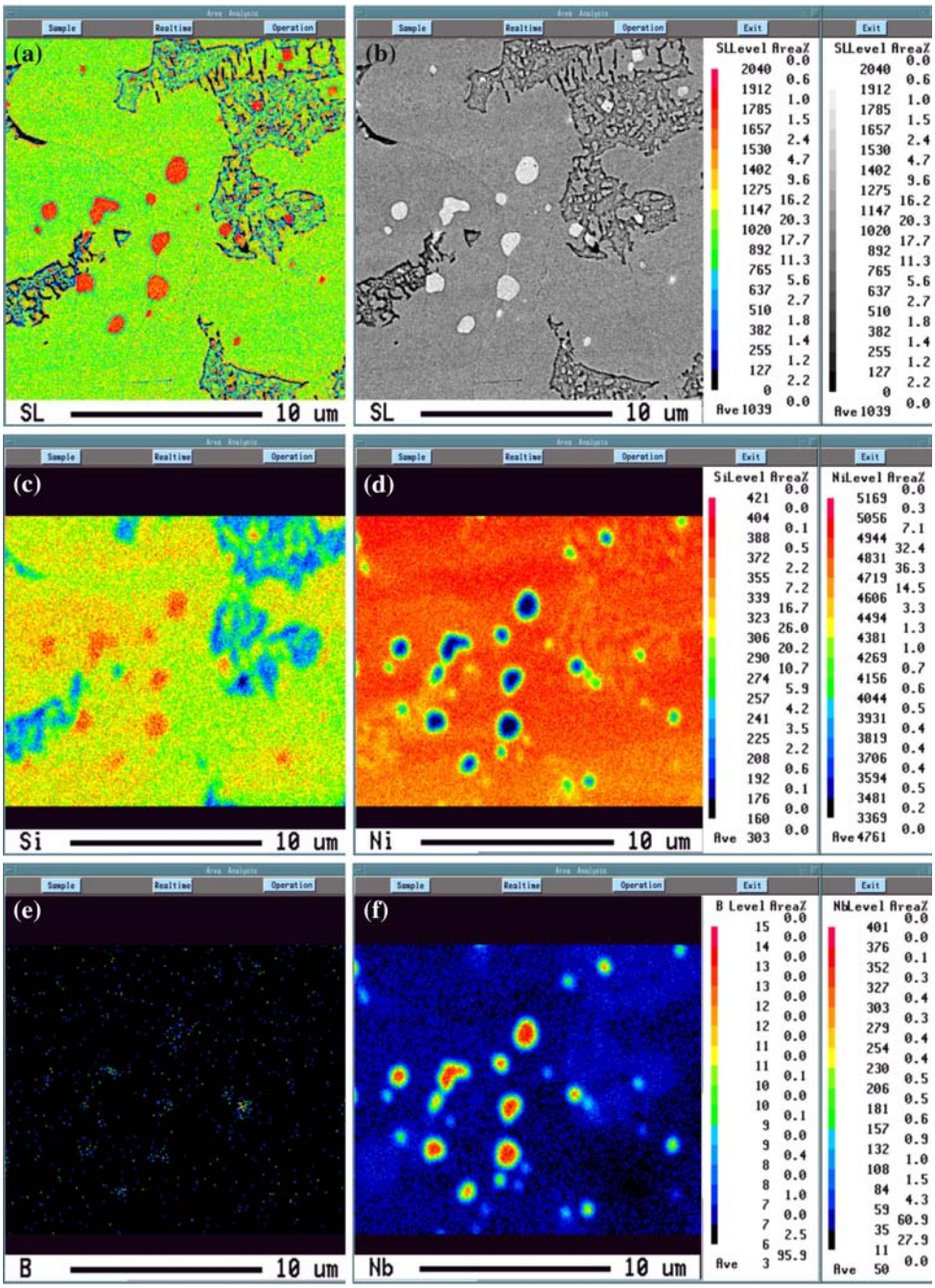

Fig. 2 EPMA images for the Ni–19Si–3Nb–0.15B–0.1C alloy; (**a**) secondary electron image, (**b**) backscattered electron image, (**c**) mapping image of Si element, (**d**) mapping image of Ni element, (**e**) mapping image of B element, (**f**) mapping image of Nb element

temperature, reaching a maximum at 873 K, and then decreases rapidly with further increase in temperature. Note that the yield stress is enhanced by 10% with the boron and carbon addition over a wide range of temperature.

The variations of the tensile elongation of the Ni–19Si–3Nb and Ni–19Si–3Nb–0.15B–0.1C alloys as a function of temperature under different environments are shown in Fig. 4. Both the Ni–19Si–3Nb alloy and Ni–19Si–3Nb–0.15B–0.1C alloys exhibit identical high elongation values (i.e. $\varepsilon > 12\%$) at room temperature under the vacuum atmosphere. In addition, the tensile elongation of Ni–19Si–3Nb–0.15B–0.1C increases slightly with increasing temperature up to 873 K, and then decreases with temperature up to 1073 K while tested in vacuum. When the unalloyed Ni–19Si–3Nb is tested in air or water vapor atmosphere, the tensile elongations are reduced to relatively low values (~5% at room temperature and <2% at 1073 K) in comparison with those obtained in vacuum. However, the Ni–19Si–3Nb–0.15B–0.1C alloy presents a significantly improvement in the tensile elongation over a wide range of temperature under both air and 850 ppm water vapor atmospheres.

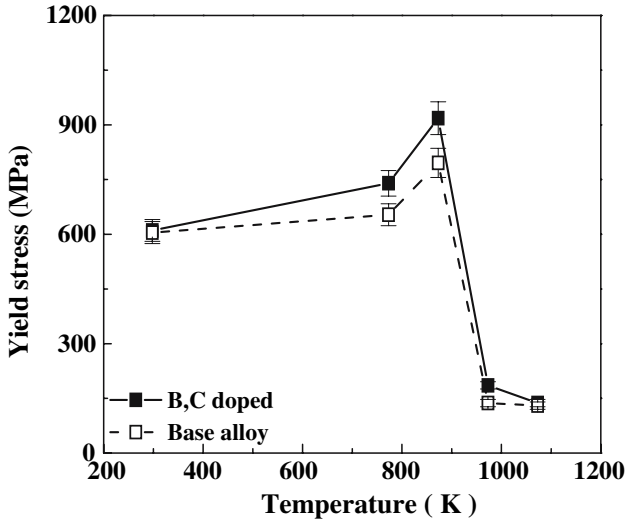

Fig. 3 Yield stress as a function of temperature for the Ni–19Si–3Nb alloy (with mark of □) and Ni–19Si–3Nb–0.15B–0.1C alloy (with mark of ■) tested in vacuum with the strain rate of 2×10^{-4} s^{-1}

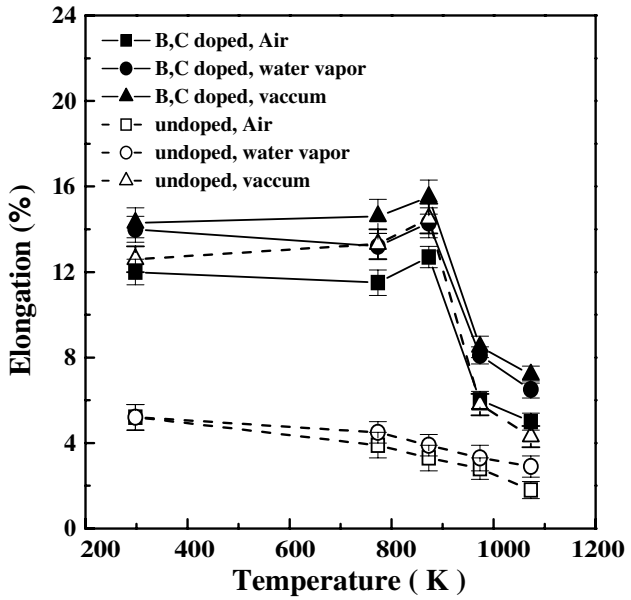

Fig. 4 Tensile elongation as a function of temperature for the Ni–19Si–3Nb alloy (with mark of □, ○, and △) and Ni–19Si–3Nb–0.15B–0.1C alloy (with mark of ■, ●,and ▲) tested in different atmosphere with the strain rate of 2×10^{-4} s^{-1}

The variations of the ultimate tensile strength (UTS) as a function of temperature for both the Ni–19Si–3Nb and the Ni–19Si–3Nb–0.15B–0.1C alloys are shown in Fig. 5. Both alloys attain high UTS values (i.e. > 1200 MPa) at room temperature when tested in vacuum. In addition, the tensile strength of these two alloys also increases with temperature up to 873 K, and then decreases with temperature up to 1073 K while tested in vacuum. As for the

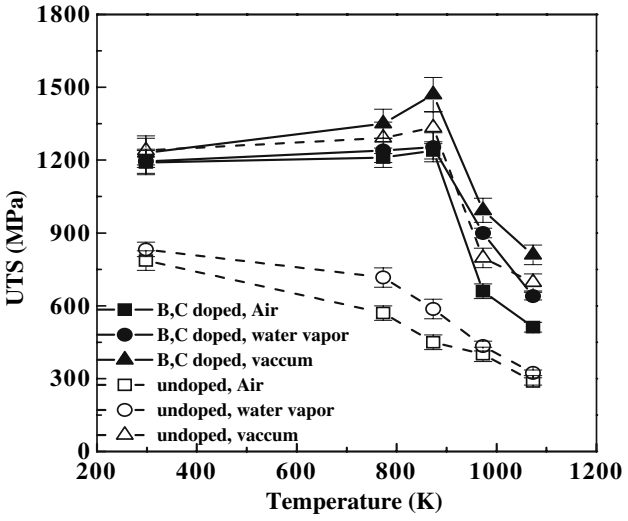

Fig. 5 Ultimate tensile strength and elongation as a function of temperature for the Ni–19Si–3Nb alloy (with mark of □, ○, and △) and Ni–19Si–3Nb–0.15B–0.1C alloy (with mark of ■, ●, and ▲) tested in different atmosphere

tests in air and 850 ppm water vapor, the Ni–19Si–3Nb–0.15B–0.1C alloy exhibits much higher UTS values than the Ni–19Si–3Nb alloy over the entire temperature range. The measured UTS data on both Ni–19Si–3Nb and Ni–19Si–3Nb–0.15B–0.1C appear to be well correlated with the results of tensile elongation.

Effects of strain rate on the tensile properties

The variations of UTS as a function of strain rate for the Ni–19Si–3Nb–0.15B–0.1C alloy tested in different atmospheres and at different temperatures are shown in Fig. 6. Both the UTS and the elongation values exhibit a similar trend to sustain relatively high values from room temperature up to 873 K, then to drop significantly up to 1073 K. In parallel, both UTS and elongation reveals a quite insensitive trend with increasing strain rate as tested at temperatures below 873 K, as shown in Fig. 6(a–c). However, the UTS exhibits a certain level of dependence on the strain rate while tested in air at temperatures greater than 873 K, the UTS increases with increasing strain rate, as shown in Fig. 6d.

Fracture behavior

The SEM fractographs taken from the Ni–19Si–3Nb–0.15B–0.1C alloy fractured in vacuum and air, tested at 873 K with different strain rates (8×10^{-5} $s^{-1}$and 2×10^{-2}), are shown in Fig. 7. The fracture surfaces of the Ni–19Si–3Nb–0.15B–0.1C alloy loaded at different strain rates reveal dimpled fracture surfaces for samples tested in

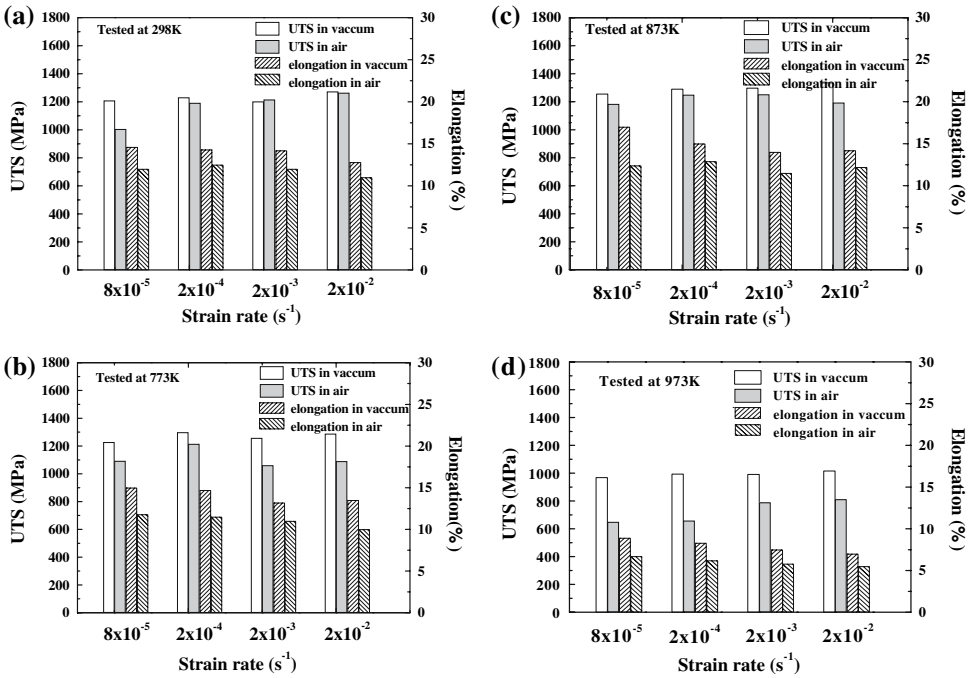

Fig. 6 Ultimate tensile strength and elongation as a function of strain rate for the Ni–19Si–3Nb–0.15B–0.1C alloy tested in air and vacuum at (**a**) 298 K, (**b**) 773 K, (**c**) 873 K, and (**d**) 973 K, respectively

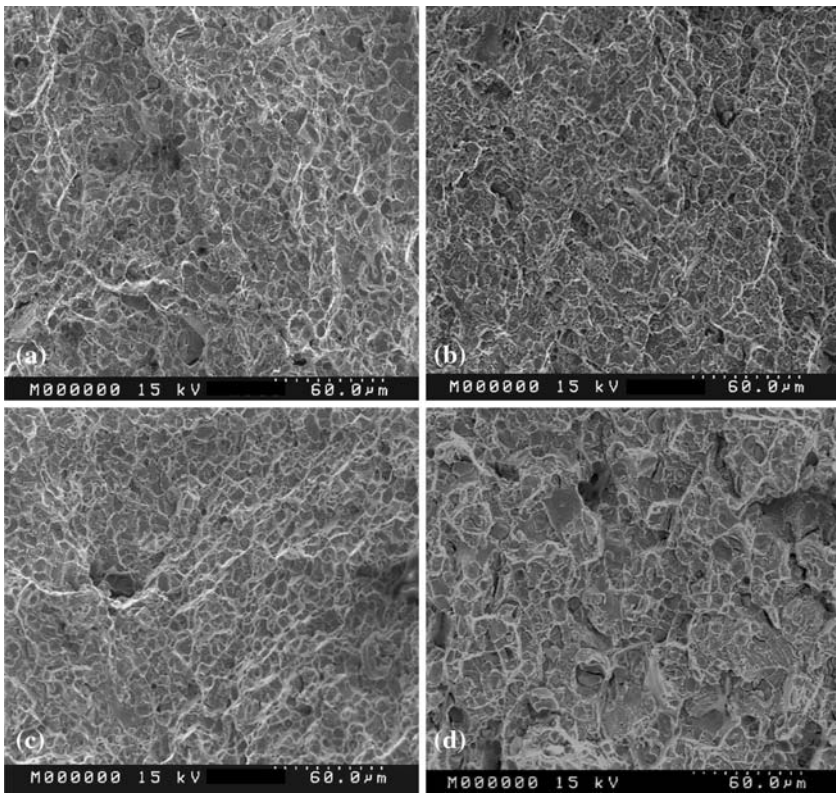

Fig. 7 SEM images of the fracture surfaces for Ni–19Si–3Nb–0.15B–0.1C alloy tested at 873 K with different strain rate; (**a**) 2×10^{-2} s^{-1} in vacuum, (**b**) 2×10^{-2} s^{-1}in air, (**c**) 8×10^{-5} s^{-1} in vacuum, (**d**) 8×10^{-5} s^{-1} in air

vacuum or in air at 873 K. The fracture mode appears to be well correlated with the measured tensile elongations. As the test temperature increases to 973 K, the fracture surface of the Ni–19Si–3Nb–0.15B–0.1C alloy still remains the dimpled fracture pattern for samples tested in vacuum at a strain rate from 2×10^{-4}, 2×10^{-3}, and 2×10^{-2}, as shown in Fig. 8(a–c). However, a clear image showing intergranular cracking mixed with partial dimpled fracture was observed on the fracture surface of the Ni–19Si–3Nb–0.15B–0.1C alloy tested at the strain rate of 2×10^{-5} s^{-1} in

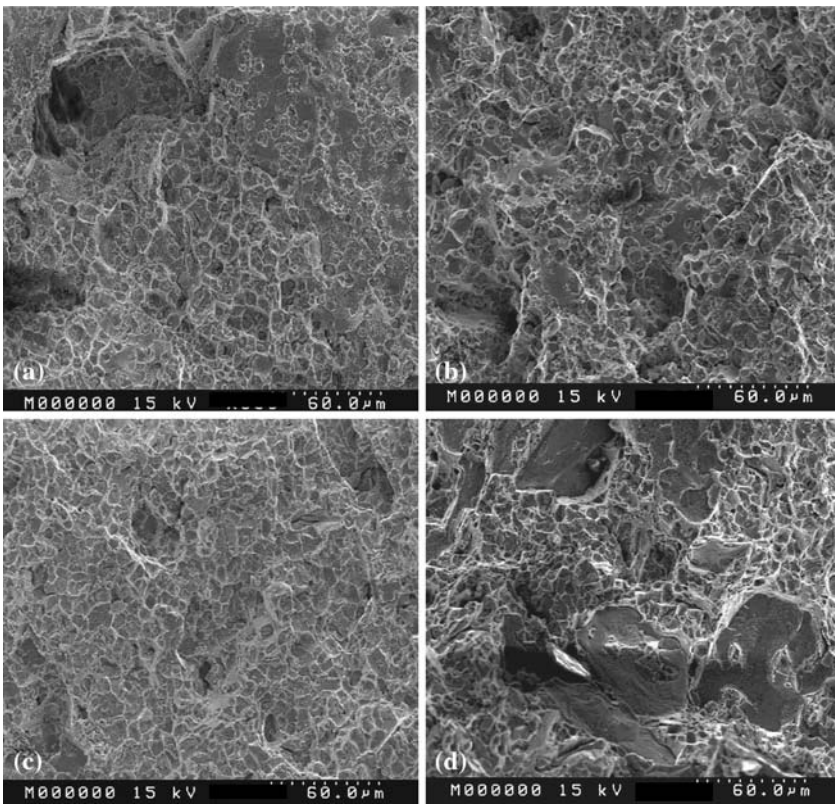

Fig. 8 SEM images of the fracture surfaces for Ni–19Si–3Nb–0.15B–0.1C alloy tested in vacuum at 973 K with different strain rate; (**a**) 2×10^{-2} s^{-1}, (**b**) 2×10^{-3} s^{-1}, (**c**) 2×10^{-4} s^{-1}, (**d**) 8×10^{-5} s^{-1}

vacuum, as shown in Fig. 8d. In addition, the fracture surface of the samples tested at 973 K with different strain rates in air presents an image of intergranular cracking mixed with a small area with dimple fracture, as shown in Fig. 9. This indicated that the addition of boron and carbon suppresses the moisture-induced embrittlement at low temperatures and becomes difficult to overcome the embrittlement at medium high temperatures (i.e. 973 K).

Discussion

The environmental effect was suggested to be associated with hydrogen-induced embrittlement at low temperatures [22–24] and oxygen-induced embrittlement at high temperatures [8, 25]. Therefore, the effect of boron addition on the suppression of environmental embrittlement could be due to the interaction between hydrogen and boron instead of the interaction between oxygen and boron in the corresponding temperature regime.

The undoped Ni–19Si–3Nb alloy actually suffers from environmental embrittlement, such as in air or in 850 ppm water vapor. This kind of environmental effect has been widely observed for a number of $L1_2$-type compounds [26–29]. It is recognized that environmental embrittlement and induced fracture involve some kinetic processes, such as decomposition, permeation and condensation of hydrogen and bond breaking processes [30–33]. Regarding the decomposition process of hydrogen, it has been proposed that materials deformed in air are embrittled due to atomic hydrogen decomposed from moisture. In addition, the active element such as Si in this alloy has been suggested to react with the moisture in air by the reaction, $Si + 2H_2O \rightarrow SiO_2 + 4H$. The generated atomic hydrogen can therefore penetrate into grain boundaries at crack tips to cause the brittle intergranular fracture. However, the results observed in the boron and carbon doped Ni–19Si–3Nb alloy clearly indicate that boron atoms suppress the environmental embrittlement in air or water vapor atmosphere at temperatures below 773 K, as shown in Figs. 4 and 5. Wang and Chung [34] have proposed that the strong B–H bonding may slow the hydrogen diffusion rate into the boron-doped $Ni_3(Al,Ti)$ (110) single crystal. This leads to a lower concentration of atomic hydrogen at the crack tip, thus can suppress hydrogen-induced embrittlement.

For the Ni–19Si–3Nb–0.15B–0.1C alloy tested in air at strain rates of 8×10^{-5} s^{-1}, 2×10^{-4}, 2×10^{-3}, and 2×10^{-2}, as the test temperature increases to the medium high temperatures (i.e. above 873 K), the ductility decreases significantly from 12% to 5.5%, as shown in Fig. 6(a, b), respectively. However, this feature is not evident in the Ni–19Si–3Nb–0.15B–0.1C alloy tested both in vacuum and in water vapor atmosphere, the elongation of the Ni–19Si–3Nb–0.15B–0.1C alloy still remains above 7%. This could

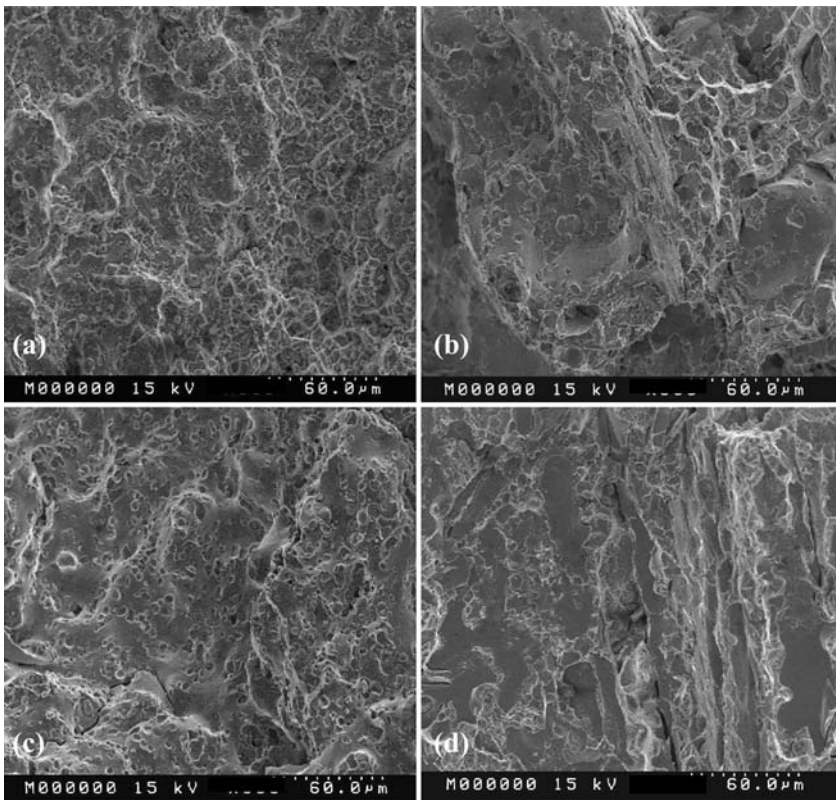

Fig. 9 SEM images of the fracture surfaces for Ni–19Si–3Nb–0.15B–0.1C alloy tested in air at 973 K with different strain rate; (**a**) 2×10^{-2} s^{-1}, (**b**) 2×10^{-3} s^{-1}, (**c**) 2×10^{-4} s^{-1}, (**d**) 8×10^{-5} s^{-1}

be the evidence of the oxygen induced embrittlement at medium high temperatures as proposed by Pike and Liu [19] and Zhu and Liu [20]. Zhu and Liu [20] proposed that the oxygen will diffuse along the grain boundary to induce dynamic embrittlement at the intermediate high temperature (such as 873 K). If the temperature is too low, the diffusion of oxygen will be too slow without noticeable oxygen penetration into the interior. Therefore, the loss in ductility at high temperatures (above 873 K) would accompany by a change in fracture mode from transgranular to intergranular which is similar to those obtained in the boron-doped Ni_3Al alloys [25] and the boron-doped $Ni_3(Si,Ti)$ alloys [12].

Conclusion

The tensile properties of the Ni–19Si–3Nb and the Ni–19Si–3Nb–0.15B–0.1C alloys are evaluated at the testing temperatures from room temperature to 1073 K under atmosphere of vacuum or air or 850 ppm water vapor with tensile strain rates of 8×10^{-5} s^{-1}, 2×10^{-4}, 2×10^{-3}, and 2×10^{-2}, respectively. The results of this study are summarized below:

(1) The microalloying of boron and carbon in the Ni–19Si–3Nb base alloy indeed improves its tensile elongation from room temperature to 873 K either in air or in water vapor atmosphere. In addition, the UTS values of these alloys appear to be well correlated with the tensile elongation data as well as the fracture mode.

(2) The addition of 0.15 at% boron and 0.1 at% carbon to the Ni–19Si–3Nb alloy results in complete suppression of moisture embrittlement in air and water vapor at temperatures from room temperature to 873 K. However, the boron and carbon doped alloy still suffers from embrittlement associated with oxygen at medium high temperatures, for instance at 973 K.

(3) Both of UTS and elongation exhibit quite insensitive dependence to the loading strain rate when tested at temperatures below 873 K. However, the UTS exhibits a highly depending trend on the strain rate when tested in air at temperatures above 873 K; the UTS increases with increasing strain rate.

Acknowledgement The authors would like to gratefully acknowledge the sponsorship from the National Science Council of ROC under the project NSC93-2745-E-214-001.

References

1. Davis RG, Stoloff NS (1965) Trans TMS-AIME, 233:714
2. Kumar KS (1995) In: Westbrook JH, Fleischer RL (eds) Intermetallic compounds-principle and practice, vol 2. John Wiley &Sons Ltd, Chichester, UK, pp 211–235
3. Evans TE, Hart AC (1971) Electrochem Acta 16:1955

4. Grala EM (1960) Mechanical properties of intermetallic compounds. Wiley, New York, p 358
5. Takasugi T, Shindo D, Izumi O, Hirabayashi M (1990) Acta Metall 38:739
6. Takasugi T, Nagashima M, Izumi O (1990) Acta Metall 38:747
7. Baker I, Yuan J, Schulson EM (1993) Metall Trans A 24A:283
8. Oliver WC (1989) In: Liu CT et al (eds) High temperature ordered intermetallic alloys III, vol 133. MRS Symposium Proceeding, Pittsburgh, PA, pp 397–402
9. Jang JSC, Tsau CH (1992) Mater Sci Eng A153:525
10. Takasugi T (2000) J Intermetallics 8:575
11. Takasugi T, Izumi O, Yoshida M (1991) J Mater Sci 26:1173; DOI 10.1007/BF00544451
12. Takasugi T, Suenaga H, Izumi O (1991) J Mater Sci 26:1179; DOI 10.1007/BF00544452
13. Liu CT, George EP, Oliver WC (1996) J Intermetallics 4:77
14. Jang JSC, Wong SK, Lee PY (2000) Mater Sci Eng A281:17
15. Jang JSC, Cheng CY, Wong SK (2001) Mater Chem Phys 72:66
16. Jang JSC, Ou CJ, Cheng CY (2002) Mater Sci Eng A329–331C:453
17. Takasugi T, Ma CL, Hanada S (1995) Mater Sci Eng A192/193:407
18. Heatherly L, George EP, Liu CT, Kumar KS (1998) Mater Sci Eng A245:80
19. Pike LM, Liu CT (2000) Scripta Mater 42:265
20. Zhu JH, Liu CT (2002) Intermetallics 10:309
21. Varin RA, Song YK (2001) J Intermetallics 9:647
22. Liu CT (1986) In: Stoloff NS, Koch CC, Liu CT, Izumi O (eds) High-temperature order intermetallic alloys II, vol 81. MRS Symposium, Pittsburgh, pp 355–367
23. Izumi O, Takasugi T (1988) J Mater Res 3:426
24. Stoloff NS (1988) J Metals 40(12):18
25. Liu CT, White CL (1987) Acta Metall 35:643
26. Liu CT, Mckamey CG, Lee EH (1990) Scripta Metall 24:385
27. Liu CT, George EP (1990) Scripta Metall 24:1285
28. George EP, Liu CT, Lin H, Pope DP (1995) Mater Sci Eng A 192/193:277
29. Takasugi T, Izumi O (1986) Acta Metall 34:607
30. Liu CT (1992) In: Liu CT et al (eds) Ordered intermetallics-physical metallurgy and mechanical behavior. Kluwer Academic Publishers, pp 321
31. George EP, Liu CT (1997) In: Nathal MV et al (eds) Structural intermetallics 1997. TMS, Warrendale, USA, pp 693–702
32. Liu CT, Lee EH, Mckamey CG (1989) Scripta Metall 23:875
33. Stoloff NS, Liu CT (1994) J Intermetallics 2:75
34. Wang J, Chung YW (2001) J Intermetallics 9:349